

Size dictated thermal conductivity of GaN

Thomas E. Beechem, Anthony E. McDonald, Elliot J. Fuller, A. Alec Talin, Christina M. Rost, Jon-Paul Maria, John T. Gaskins, Patrick E. Hopkins, and Andrew A. Allerman

Citation: [Journal of Applied Physics](#) **120**, 095104 (2016); doi: 10.1063/1.4962010

View online: <http://dx.doi.org/10.1063/1.4962010>

View Table of Contents: <http://scitation.aip.org/content/aip/journal/jap/120/9?ver=pdfcov>

Published by the [AIP Publishing](#)

Articles you may be interested in

[Suppression of thermal conductivity in \$\text{In}_x\text{Ga}_{1-x}\text{N}\$ alloys by nanometer-scale disorder](#)

Appl. Phys. Lett. **102**, 121906 (2013); 10.1063/1.4798838

[Anisotropic Mg incorporation in GaN growth on nonplanar templates](#)

Appl. Phys. Lett. **86**, 121901 (2005); 10.1063/1.1870121

[Ion-beam processing effects on the thermal conductivity of n-GaN/sapphire \(0001\)](#)

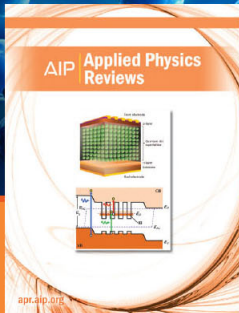
J. Appl. Phys. **91**, 1277 (2002); 10.1063/1.1428798

[High spatial resolution thermal conductivity and Raman spectroscopy investigation of hydride vapor phase epitaxy grown n - GaN/sapphire \(0001\): Doping dependence](#)

J. Appl. Phys. **88**, 3295 (2000); 10.1063/1.1289072

[Optical microscopy of electronic and structural properties of epitaxial laterally overgrown GaN](#)

Appl. Phys. Lett. **74**, 3320 (1999); 10.1063/1.123331



NEW Special Topic Sections

NOW ONLINE
Lithium Niobate Properties and Applications:
Reviews of Emerging Trends

AIP | Applied Physics Reviews

Size dictated thermal conductivity of GaN

Thomas E. Beechem,^{1,a)} Anthony E. McDonald,¹ Elliot J. Fuller,² A. Alec Talin,² Christina M. Rost,³ Jon-Paul Maria,³ John T. Gaskins,⁴ Patrick E. Hopkins,⁴ and Andrew A. Allerman¹

¹Sandia National Laboratories, Albuquerque, New Mexico 87123, USA

²Sandia National Laboratories, Livermore, California 94551, USA

³Department of Materials Science and Engineering, North Carolina State University, Raleigh, North Carolina 27695, USA

⁴Department of Mechanical and Aerospace Engineering, University of Virginia, Charlottesville, Virginia 22904, USA

(Received 14 April 2016; accepted 18 August 2016; published online 2 September 2016)

The thermal conductivity of n- and p-type doped gallium nitride (GaN) epilayers having thicknesses of 3–4 μm was investigated using time domain thermoreflectance. Despite possessing carrier concentrations ranging across 3 decades (10^{15} – 10^{18} cm^{-3}), n-type layers exhibit a nearly constant thermal conductivity of 180 W/mK. The thermal conductivity of p-type epilayers, in contrast, reduces from 160 to 110 W/mK with increased doping. These trends—and their overall reduction relative to bulk—are explained leveraging established scattering models where it is shown that, while the decrease in p-type layers is partly due to the increased impurity levels evolving from its doping, size effects play a primary role in limiting the thermal conductivity of GaN layers tens of microns thick. Device layers, even of pristine quality, will therefore exhibit thermal conductivities less than the bulk value of 240 W/mK owing to their finite thickness. *Published by AIP Publishing.* [<http://dx.doi.org/10.1063/1.4962010>]

I. INTRODUCTION

Owing to its wide bandgap, chemical stability, and comparatively high mobility, gallium nitride (GaN) is commercially established for applications in solid state lighting,¹ defense, and communications.² It is also being increasingly pursued for use in power electronics where its large breakdown field may offer enhanced efficiency in smaller packages.³ Regardless of application, heightened operating temperature is of pernicious influence diminishing not only lifetime but also performance.^{4–6} Parameters determining the operating temperature—including the thermal conductivity of the GaN itself—therefore dictate the capability.

The thermal conductivity of a crystalline semiconductor is dictated by interatomic bonding defining the phonon dispersion and sources of scattering impeding the flux of these phonons. Under ideal conditions, the same strong interatomic bonds that give GaN its wide-bandgap also lead to a thermal conductivity that is nearly twice that of silicon at room temperature.⁷ Device layers are not ideal, however. Electronic functionality demands the inclusion of phonon scattering sources. Dopants used to modify the electronic carrier concentration, for instance, cause impurity scattering. Heteroepitaxy providing scalability also imbues dislocations that impede the flow of phonons. The finite thickness of the layers (1–20 μm (Refs. 8–11)) themselves induce boundary scattering. Taken together, the thermal conductivity of a GaN device layer is therefore defined not by the intrinsic material characteristics but rather by the interplay of these extrinsic scattering sources. Here, the relative strength of these sources is investigated.

From a quantitative perspective, measurements^{12,13} and first principles calculations⁷ have shown that the thermal conductivity of thick (≥ 100 μm) high-quality GaN is between 230 and 250 W/mK at 300 K. The inclusion of dopants or impurities present in some device layers ($n_{\text{Imp}} \sim 1 \times 10^{20}$ cm^{-3}), however, reduces this value by nearly $2\times$.^{14–16} Dislocation densities not uncommon in the devices ($N_D \sim 5 \times 10^8$ cm^{-2}),³ meanwhile, cause a similar degradation.^{17,18} Beyond the effects of impurities and dislocations, the finite thickness of a GaN device layer will also lessen the thermal conductivity. Numerous studies have shown that when the mean free path (MFP) of heat carrying phonons is comparable to the layer thickness, boundary scattering inhibits heat transport.¹⁹ In GaN, over half the heat is carried by phonons having a mean free path on the order of 1 μm .²⁰ Since most GaN device layers have thicknesses on this scale, size effects will therefore impact the thermal conductivity.

Despite this general understanding, the impact of layer thickness on the thermal conductivity of GaN has not been addressed explicitly; this is our aim. To this end, thin (3–4 μm) GaN epilayers having free carrier concentrations of varying level ($\leq 10^{16}$ – 10^{18} cm^{-3}) and type (n and p) were measured utilizing time domain thermoreflectance (TDTR). By interpreting the results with established scattering models accounting for dislocations, impurities, and boundaries, size effects are shown to dictate the thermal conductivity of GaN layers of reasonable purity ($n_{\text{Imp}} \leq 5 \times 10^{18}$ cm^{-3}) and quality ($N_D < 1 \times 10^8$ cm^{-2}) even when tens of microns thick.

II. SYNTHESIS AND CHARACTERIZATION

GaN epilayers (3–4 μm) were synthesized via metalorganic chemical vapor deposition (MOCVD) in a Veeco

^{a)}Electronic mail: tebeech@sandia.gov

D-125 system at 200 Torr. Trimethylgallium (TMGa) and ammonia provided the group-III and group-V elements, respectively, while silane and bis(cyclopentadienyl)magnesium (Cp_2Mg) were used as dopant sources. Epitaxial growth was performed on 1 cm^2 GaN substrates grown by hydride vapor phase epitaxy (HVPE), which were obtained commercially from Kyma Technologies. The electron concentration ($N_d - N_a$) of $4\text{ }\mu\text{m}$ thick n-type samples was determined by capacitance-voltage measurements using a mercury (Hg) probe. Hall effect measurements made on separate calibration layers were used to estimate the hole concentration of $3\text{ }\mu\text{m}$ thick p-type layers doped with Mg. Following growth, p-type layers were thermally annealed at $900\text{ }^\circ\text{C}$ for 5 min under nitrogen to activate the Mg dopants. Additional p-type epilayers were examined apart from the anneal with the results independent to this process.²¹

The HVPE substrates initially possessed dislocation densities on the order of 10^7 cm^{-2} as confirmed by cathodoluminescence (CL) on wafers from the same vendor. The MOCVD homoepitaxy results in dislocation densities equal to or slightly less than the growth substrate.^{22,23} For the epilayers considered here, order of magnitude estimates obtained from high-resolution X-Ray diffraction (HRXRD) measurements²⁴ and CL were consistent with this presumption. Variation among samples was less than $10\times$. Impurity concentrations were obtained *via* secondary ion mass spectroscopy (SIMS) with the values shown in Table I.

Room temperature thermal conductivity was measured for each film with the time domain thermoreflectance (TDTR) acquired independently in “round robin” fashion across three separate systems at Sandia National Laboratories and the University of Virginia using both two-color²⁵ and two-tint²⁶ implementations. Results among all measurements—regardless of laboratory or implementation—correlated to within the 20% uncertainty typical of TDTR. As addressed in detail previously,^{25–28} the specifics of the current implementation are briefly described below.

Each film was coated with $\sim 80\text{ nm}$ of aluminum (Al) using electron beam evaporation. Before coating, the films were cleaned in a two-step process beginning with a 3 min submersion in a 50% solution of hydrochloric acid (HCl) and deionized water (DI) followed by a 1 min submersion in a 1% hydrofluoric (HF) acid solution. After each step, a DI rinse and N_2 dry were employed. TDTR measurements utilized a $\sim 100\text{ fs}$ pulse emanating from a Ti:sapphire oscillating laser operating at 80 MHz and centered at 800 nm. Pump and probe beam sizes were focussed collinearly on the sample and ranged in diameter ($1/e^2$) from $40\text{--}60\text{ }\mu\text{m}$ and $8\text{--}20\text{ }\mu\text{m}$, respectively. Results were independent of beam size consistent with the expectation.²⁹ For two-color measurements, the pump is doubled via a 2 mm thick BiB_3O_5

crystal to 400 nm. The two-tint approach filters different spectral portions of the laser along the pump and probe paths. An electro-optic modulator (EOM) “chopped” the pump beam at frequencies of both 8.8 and 11.3 MHz with the results independent of this parameter. By fitting the ratio of the in-phase to out-of-phase thermoreflectance signal to a model explained elsewhere,^{30–33} GaN’s thermal conductivity and its interfacial conductance with the overlaying Al transducer were deduced.

To facilitate fitting, picosecond acoustics quantified the Al thickness assuming a sound velocity of 6420 m/s .³⁴ Thermal conductivity of the Al was quantified using 4-point resistivity measurements in combination with the Wiedmann-Franz law. A volumetric specific heat of $2.64\text{ J/cm}^3\text{ K}$ (Refs. 35–38) was specified for GaN and its thermal conductivity defined as isotropic.^{15,39} Uncertainty associated with an individual implementation (e.g., two-tint, two-color) of TDTR was calculated *via* previously reported procedures.^{28,40} Total uncertainty was quantified by vector summing these individual contributions with the variation observed between different laboratories and approaches. Reported values are the mean from all measurements.

III. RESULTS AND DISCUSSION

Thermal boundary conductance ranges in magnitude from 118 to $278\text{ MW/m}^2\text{ K}$ in line with the previous measurements⁴¹ independent of either type or degree of doping. Thermal conductivity, in contrast, varies with dopant type and concentration. N-type films exhibit near independence to free carrier concentration possessing an average thermal conductivity of $K_n = 180\text{ W/mK}$ as shown in Figure 1. P-type films (K_p), on the other hand, reduce from 160 W/mK to 110 W/mK with less than a decade increase in free carrier concentration. For both sets of films, the thermal conductivity is less than the bulk value of 240 W/mK despite the relatively low dislocation density. In the following, traditional models of phonon scattering are leveraged to interpret these

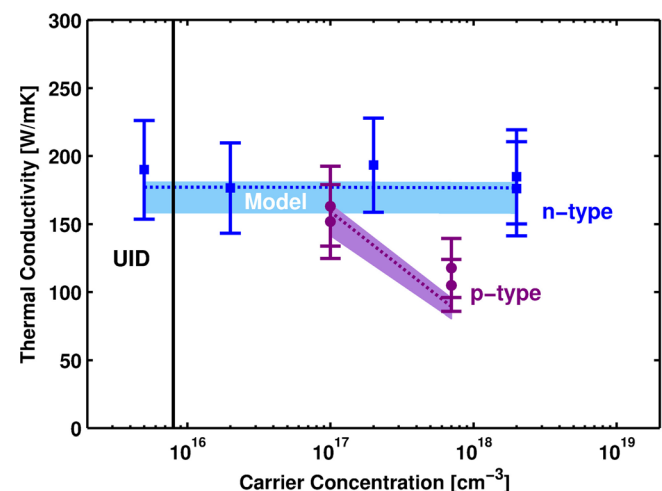


FIG. 1. Measured thermal conductivity of n-type ($4\text{ }\mu\text{m}$) and p-type ($3\text{ }\mu\text{m}$) GaN epilayers of varying free carrier concentration. Shaded boxes correlate with the predictions from Eq. (1) where the bounds are defined by the uncertainty in dislocation density and thickness. Dotted lines correspond to the mean prediction.

TABLE I. Impurity concentration in units of cm^{-3} .

Type	C	O	H	Si	Mg
n-type	3×10^{16}	3×10^{16}	3×10^{16}	$\leq 2 \times 10^{18}$	NA
p-type (low)	1×10^{17}	3×10^{16}	7×10^{17}	NA	2.5×10^{18}
p-type (high)	4×10^{16}	3×10^{16}	$1.6 - 2.5 \times 10^{19}$	NA	3×10^{19}

trends—(1) $K_{n,p} < K_{Bulk}$ (2) $K_n > K_p$, and (3) $K_{n(p)}$ independent (dependent) to carrier concentration—demonstrating the primary role that size plays in determining the thermal conductivity of micron-scale GaN.

Thermal conductivity was quantified *via*

$$k = \frac{1}{6\pi^2} \sum_s \int_0^{q_{m,s}} \frac{\hbar^2 \omega_s^2(q)}{k_B T^2} \frac{\exp\left(\frac{\hbar \omega_s(q)}{k_B T}\right)}{\left[\exp\left(\frac{\hbar \omega_s(q)}{k_B T}\right) - 1\right]^2} \times v_s^2(q) \tau_s(q) q^2 dq, \quad (1)$$

where the sum is over all polarization branches, q is the wave-vector, ω is the phonon frequency, k_B is the Boltzmann constant, \hbar is the modified Planck's constant, v is the group velocity, and τ is the scattering time. Practically, Eq. (1) was evaluated leveraging an isotropic dispersion having characteristics of the Γ -A direction where each of the polarizations—including optical branches^{42,43}—is represented by fourth order polynomial fits to the data of Ruf *et al.*⁴⁴ The scattering time was calculated including Umklapp (τ_U), impurity (τ_I), dislocation (τ_D), and boundary (i.e., size), τ_B , scattering. Electron-phonon scattering was not included as at the free carrier concentrations considered here ($n(p) < 1 \times 10^{19} \text{ cm}^{-3}$); its impact is of negligible consequence at 300 K.¹³ Supporting this approach, no difference was found in the measured thermal conductivity based on dopant activation.

Umklapp scattering was calculated through $\tau_U^{-1} = P\omega^2(q)T \exp(-C_u/T)$. The coefficients, P and C_u , were obtained by fitting the temperature dependent data of Jezowski *et al.*¹² from 100 to 300 K resulting in values of $0.99 \times 10^{-19} \text{ s/K}$ and 221 K, respectively. Impurity scattering was quantified utilizing the relation $\tau_I^{-1} = \frac{V_o \Gamma}{4\pi \bar{v}^3} \omega^4(q)$, where $V_o = \sqrt{3}a^2c/8$ is the crystal's unit volume⁴⁵ and \bar{v} is the average sound speed.⁴⁶ Γ is a term representing the strength of the scattering stemming from mass and strain perturbations induced by the impurities and was calculated from

$$\Gamma = \sum_i f_i \left[\left(1 - \frac{M_i}{\bar{M}}\right)^2 + 2 \left\{ -6.4\gamma \left(\frac{\Delta R_i}{R}\right) \right\}^2 \right], \quad (2)$$

where f_i is the fractional concentration of the i th atom species such that summing over all atomic species provides the average atomic mass of the crystal given by $\bar{M} = \sum_i f_i M_i$. Isotopic scattering is included in this term by accounting for the natural distributions of Ga⁶⁹ (60%), Ga⁷¹ (40%), N¹⁴ (99.6%), and N¹⁶ (0.4%).¹⁶ $\frac{\Delta R_i}{R}$ is the variation of strain induced in the crystal lattice induced by the i th species as quantified using Pauling ionic radii.^{47,48} It was assumed that Mg and Si formed substitutional defects on Ga sites, whereas C and O integrated into the lattice at N sites. Hydrogen was specified as an interstitial.⁴⁹

Scattering from dislocations was evaluated from $\tau_D^{-1} = \psi(\tau_{DC}^{-1} + \tau_S^{-1} + \tau_E^{-1} + \tau_M^{-1})$ where the terms in the parentheses correspond to the dislocation cores and the strain fields associated with screw, edge, and mixed dislocations, respectively. These terms were evaluated using the approach of Zou *et al.*⁴⁷ ψ is a dimensionless empirical parameter

stipulated to be 1000. Physically, an increase in ψ can be viewed as an adjustment to the Klemens formulation—known to underpredict by two to three orders of magnitude for a variety of materials^{50–54}—to more accurately account for heightened anharmonicity imbued to the crystal by the dislocations.⁵⁵ Practically, the use of ψ induces reductions in the thermal conductivity of GaN at densities $\sim 10^8 \text{ cm}^{-2}$ in line with Mion *et al.*¹⁷ even when the size effects are deconvolved from their results.

The mean free path of phonons (MFP) in semiconductors ranges from nanometers to hundreds of microns in extent.^{56,57} For this reason, as a material's thickness approaches these length scales phonon scattering increases relative to bulk. Increased scattering, in turn, reduces the thermal conductivity. To assess the impact of such scattering, size effects are examined by calculating the total scattering time, $\tau_s(q)$, in Eq. (1) *via*

$$\frac{1}{\tau_s(q)} = \frac{1}{\tau_o(q)} + \frac{v(q)}{FL}, \quad (3)$$

where L is the thickness of the sample and F is a non-dimensional parameter equal to 2.38 found by fitting the form of this equation to the Boltzmann solution for a film as delineated by Dingle.⁵⁸ This form is analogous to that utilized for size effects by Yang and Dames⁵⁷ in nanowires. $\tau_o(q)$ is a “bulk” scattering term deduced from Matthiessen's rule, $\tau_o^{-1} = \tau_U^{-1} + \tau_I^{-1} + \tau_D^{-1}$. Together, Equations (1)–(3) provide a means to calculate the thermal conductivity where fitting is used only to define the nature of phonon-phonon scattering intrinsic to the material (i.e., not sample dependent).

The shaded boxes in Figure 1 were calculated with the above methodology where the bounds result from assuming a dislocation density ranging from 10^6 to 10^8 cm^{-2} and a thickness of $\pm 200 \text{ nm}$. The broad range of dislocation density is overly conservative but highlights the relatively benign impact of this parameter for the thin films considered here. This will be further discussed subsequently. For both the p and n-type films, the prediction correlates well with the experimental results. Specifically, the model accurately describes the near constancy in the thermal conductivity of the n-type films with free carrier concentration in contrast to the reduction observed in the p-type epilayers. Owing to this correlation, analysis of the scattering terms thus provides a keyhole through which to interpret the experimental trends observed here and those published previously.

To this end, Figure 2 plots GaN's thermal conductivity as a function of thickness, dislocation, and impurity density as calculated *via* Eq. (1). When not the variable of interest, an impurity concentration of 10^{16} cm^{-3} was specified for all elemental species (Figures 2(a) and 2(b)). Similarly, when assessing the impact of size and impurities, a dislocation density of 10^4 cm^{-2} was dictated (Figures 2(a) and 2(c)). Since at these levels neither impurities nor dislocations are of consequence, Figure 2 thus identifies the “pain point” when each individual parameter begins to degrade thermal conductivity. For example, Figure 2(b) highlights that thermal conductivity is impervious to dislocations up to a level of 10^8 cm^{-2} . Impurities are not of consequence until

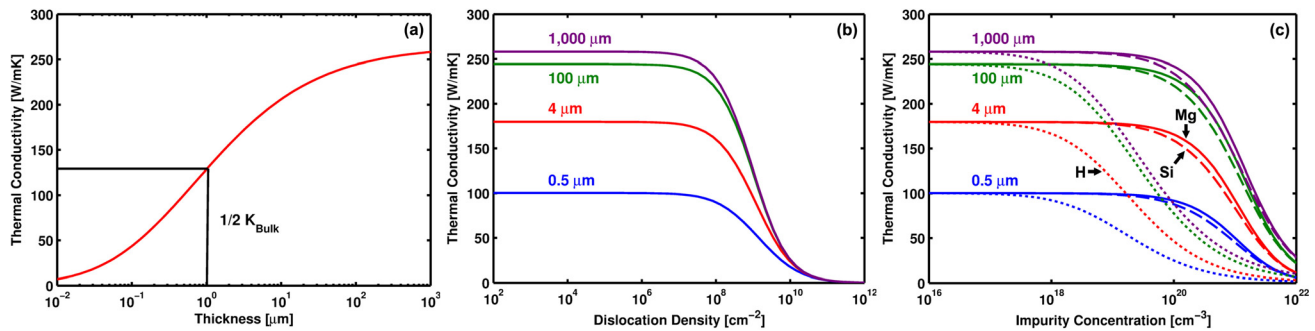


FIG. 2. Thermal conductivity as a function (a) sample thickness, (b) dislocation density, and (c) impurity concentration. In (c), solid lines correspond to thermal conductivity versus Mg concentration while the dashed and dotted lines represent Si and H, respectively.

reaching levels in excess of 10^{18} cm^{-3} in the case of H and 10^{20} cm^{-3} for Si and Mg (see Figure 2(c)).

For the more highly doped p-type films, the H concentration exceeds this threshold value whereas those more lightly doped reside comfortably below (see Table I). Thermal conductivity thus reduces with increased doping for the p-type films due to impurity scattering. The n-type films, in contrast, possess impurity levels (i.e., Si) below that impacting thermal conductivity even when highly doped. Consequently, n-type samples are unaffected by impurities and exhibit a thermal conductivity independent to carrier concentration (see Figure 1). Thermal conductivity remains reduced relative to bulk, however, despite the comparatively low impurity and dislocation densities. For this reason, the size effects are subsequently examined.

Size induces a 10% reduction in conductivity when the GaN layer becomes less than $40 \mu\text{m}$. Similar to that predicted by Freedman *et al.*,²⁰ a 50% reduction occurs for films $1 \mu\text{m}$ thick. For the 3–4 μm thick epilayers considered here, Figure 2(a) indicates that even with pristine GaN a thermal conductivity of only 170–180 W/mK can be expected. The n-type epilayers possess dislocation densities of $\sim 10^7 \text{ cm}^{-2}$ and a maximum impurity concentration of $< 2 \times 10^{18} \text{ cm}^{-3}$. From the perspective of thermal transport as outlined in Figure 2, they are pristine. The observed average value of 180 W/mK is, therefore, dictated by the very size of the film. The p-type layers, in contrast, are not pristine. Compensation requires additional magnesium and hydrogen for similar carrier concentrations relative to the amount of silicon needed for n-type doping. For example, a carrier concentration of $7 \times 10^{17} \text{ cm}^{-3}$ resulted in impurity concentrations of $> 1 \times 10^{19} \text{ cm}^{-3}$ for both Mg and H in the p-type films compared to $\leq 2 \times 10^{18} \text{ cm}^{-3}$ for the n-type epilayers (see Table I). Therefore, with increasing doping, the thermal conductivity of the p-type epilayers reduces from its size limited value of 170 W/mK to its size and impurity determined value of 110 W/mK (see Figure 2(c)). Even in the highly doped p-type epilayer, however, size plays an important role in the determination of thermal conductivity, causing a reduction on par with that of the dopant atoms.

The role of size is not only apparent in the films considered here but in the previously published thermal conductivity values of GaN in aggregate. Figure 3 provides the measured room temperature values of GaN thermal conductivity as a function of sample thickness for the past ~ 40 years since the original report of Sichel and Pankove.³⁹ An

increasing trend with thickness is clearly apparent as highlighted by the dashed curve. This curve is merely a guide to the eye, however, as the composite data represents GaN possessing disparate degrees of dislocations and impurities. To then quantitatively orient the impact of size, dislocations, and impurities, contours are provided in Figure 3. These contours plot the thermal conductivity as a function of thickness for a given dislocation density over a Si-based impurity concentration spanning 10^{16} to 10^{20} cm^{-3} . While most studies do not provide the requisite information for direct comparison to the contours, trends are generally consistent with the expectation in which thicker films rest in contours of lower dislocation density.¹⁷

Using Figure 3 as a heuristic linking sample characteristics to conductivity, implications on the thermal properties of device layers emerge. First, the architecture of both lateral high electron mobility transistors (HEMT) in which the GaN is typically $2 \mu\text{m}$ thick and power diodes possessing thicknesses of $20 \mu\text{m}$ dictates that a bulk thermal conductivity will not be realized even if made of “perfect” GaN. Rather, thermal conductivities less than 200 W/mK are more likely. No film less than $100 \mu\text{m}$ has been reported to have a thermal conductivity greater than 215 W/mK. Second, compensation of intrinsic doping using counter-doping implants is benign to thermal transport as long as total impurity levels remain below 10^{19} cm^{-3} . Third, the impact of doping and dislocations on

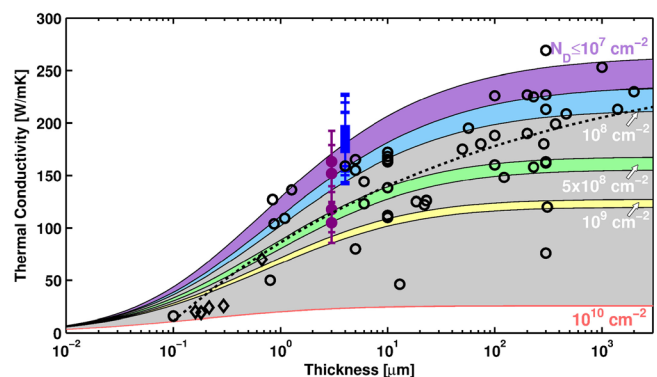


FIG. 3. Thickness dependent thermal conductivity of GaN at varying (colored bands) dislocation densities and impurity levels compared to (symbols) the published values of GaN’s thermal conductivity.^{12–18,39,59–70} Filled symbols are from the present effort. Diamonds correspond to GaN nanowires. Dotted line is guide to the eye. All values correspond to a measurement temperature of $\sim 300 \text{ K}$.

thermal conductivity lessens as the device layer becomes thinner. It is size instead that dictates the thermal transport.

IV. CONCLUSIONS

From measurements of epilayer films having varying free carrier concentration, size effects are shown to dominate the thermal conductivity of GaN. Quantitatively, GaN's thermal conductivity reduces by half relative to its bulk value for films 1 μm in thickness. GaN device layers are typically on this order and will therefore exhibit thermal conductivities reduced relative to the bulk values even if of pristine quality. Fully capitalizing upon the large intrinsic thermal conductivity of the material is therefore unlikely in current device architectures.

ACKNOWLEDGMENTS

A critical review of this work by Kimberlee C. Collins of Sandia National Laboratories is greatly appreciated. A special thanks to Karen Cross for her work in preparing the metal transducers used in TDTR measurements. This work was supported by the LDRD program at Sandia National Laboratories (SNL). Sandia National Laboratories is a multiprogram laboratory managed and operated by Sandia Corporation, a wholly owned subsidiary of Lockheed Martin Corporation, for the U.S. DOE National Nuclear Security Administration under Contract No. DE-AC04-94AL85000. J.T.G. and P.E.H. appreciate the funding from the National Science Foundation, Grant No. EECs-1509362. J-P. M. and C.M.R. acknowledge support from the NSF under contract DME-1508191.

- ¹S. Nakamura, *Rev. Mod. Phys.* **87**, 1139 (2015).
- ²J. J. Komiak, *IEEE Microwave Mag.* **16**, 97 (2015).
- ³F. Iacopi, M. Van Hove, M. Charles, and K. Endo, *MRS Bull.* **40**, 390 (2015).
- ⁴A. Christensen and S. Graham, *Appl. Therm. Eng.* **29**, 364 (2009).
- ⁵D. Green, B. Vembu, D. Hepper, S. Gibb, D. Jin, R. Vetry, J. R. Shealy, T. Beechem, and S. Graham, *Phys. Status Solidi C* **5**, 2026 (2008).
- ⁶T. C. Kizilyalli, P. Bui-Quang, D. Disney, H. Bhatia, and O. Aktas, *Microelectron. Reliab.* **55**, 1654 (2015).
- ⁷L. Lindsay, D. A. Broido, and T. L. Reinecke, *Phys. Rev. Lett.* **109**, 095901 (2012).
- ⁸H. Ji, M. Kuball, A. Sarua, A. Jo Das, W. A. Ruythooren, M. A. Germain, and G. A. Borghs, *IEEE Trans. Electron Devices* **53**, 2658 (2006).
- ⁹T. Beechem, A. Christensen, S. Graham, and D. Green, *J. Appl. Phys.* **103**, 124501 (2008).
- ¹⁰J. R. Dickerson, A. A. Allerman, B. N. Bryant, A. J. Fischer, M. P. King, M. W. Moseley, A. M. Armstrong, R. J. Kaplar, I. C. Kizilyalli, and O. Aktas, *IEEE Trans. Electron Devices* **63**, 419 (2016).
- ¹¹H. Ohta, N. Kaneda, F. Horikiri, Y. Narita, T. Yoshida, T. Mishima, and T. Nakamura, *IEEE Electron Device Lett.* **36**, 1180 (2015).
- ¹²A. Jezowski, B. A. Danilchenko, M. Bockowski, I. Grzegory, S. Krukowski, T. Suski, and T. Paszkiewicz, *Solid State Commun.* **128**, 69 (2003).
- ¹³A. Jezowski, O. Churiukova, J. Mucha, T. Suski, I. A. Obukhov, and B. A. Danilchenko, *Mater. Res. Express* **2**, 085902 (2015).
- ¹⁴D. Florescu, V. Asnin, F. H. Pollak, R. Molnar, and C. Wood, *J. Appl. Phys.* **88**, 3295 (2000).
- ¹⁵G. A. Slack, L. J. Schowalter, D. Morelli, and J. A. Freitas, Jr., *J. Cryst. Growth* **246**, 287 (2002).
- ¹⁶R. B. Simon, J. Anaya, and M. Kuball, *Appl. Phys. Lett.* **105**, 202105 (2014).
- ¹⁷C. Mion, J. Muth, E. Preble, and D. Hanser, *Appl. Phys. Lett.* **89**, 092123 (2006).
- ¹⁸Z. Su, L. Huang, F. Liu, J. P. Freedman, L. M. Porter, R. F. Davis, and J. A. Malen, *Appl. Phys. Lett.* **100**, 201106 (2012).
- ¹⁹A. M. Marconnet, M. Asheghi, and K. E. Goodson, *J. Heat Transfer* **135**, 061601 (2013).
- ²⁰J. P. Freedman, J. H. Leach, E. A. Preble, Z. Sitar, R. F. Davis, and J. A. Malen, *Sci. Rep.* **3**, 2963 (2013).
- ²¹Non-annealed films are plotted subsequently assuming an effective carrier concentration that would be expected after activation.
- ²²J. Freitas, M. Mastro, E. Imhoff, M. Tadjer, C. Eddy, and F. Kub, *J. Cryst. Growth* **312**, 2616 (2010).
- ²³C. R. Miskys, M. K. Kelly, O. Ambacher, G. Martínez-Criado, and M. Stutzmann, *Appl. Phys. Lett.* **77**, 1858 (2000).
- ²⁴Dislocation densities were estimated through omega rocking-curve measurements around the (002) GaN peak using a PANalytical Empyrean diffractometer with Cu K-alpha radiation. Incident beam optics consisted of a double-bounce Ge hybrid monochromator fitted with a $1/32^\circ$ divergence slit. A parallel plate collimator (0.18°) with a Xe proportional counter detector served as diffracted beam optics. Measurement step size was 0.001° with a 0.5 s count time per step.
- ²⁵A. J. Schmidt, "Optical characterization of thermal transport from the nanoscale to the macroscale," Ph.D. thesis, Massachusetts Institute of Technology, 2008.
- ²⁶K. Kang, Y. K. Koh, C. Chiritescu, X. Zheng, and D. G. Cahill, *Rev. Sci. Instrum.* **79**, 114901 (2008).
- ²⁷C. S. Gorham, K. Hattar, R. Cheaito, J. C. Duda, J. T. Gaskins, T. E. Beechem, J. F. Ihlefeld, L. B. Biedermann, E. S. Piekos, D. L. Medlin, and P. E. Hopkins, *Phys. Rev. B* **90**, 024301 (2014).
- ²⁸C. D. Landon, R. H. T. Wilke, M. T. Brumbach, G. L. Brennecke, M. Blea-Kirby, J. F. Ihlefeld, M. J. Marinella, and T. E. Beechem, *Appl. Phys. Lett.* **107**, 023108 (2015).
- ²⁹R. B. Wilson and D. G. Cahill, *Appl. Phys. Lett.* **107**, 203112 (2015).
- ³⁰D. G. Cahill, *Rev. Sci. Instrum.* **75**, 5119 (2004).
- ³¹A. J. Schmidt, X. Chen, and G. Chen, *Rev. Sci. Instrum.* **79**, 114902 (2008).
- ³²J. Zhu, D. Tang, W. Wang, J. Liu, K. W. Holub, and R. Yang, *J. Appl. Phys.* **108**, 094315 (2010).
- ³³P. E. Hopkins, J. R. Serrano, L. M. Phinney, S. P. Kearney, T. W. Grasser, and C. T. Harris, *J. Heat Transfer* **132**, 081302 (2010).
- ³⁴W. M. Haynes, *CRC Handbook of Chemistry and Physics* (CRC Press, 2014).
- ³⁵J. Leitner, A. Strejc, D. Sedmidubský, and K. Růžička, *Thermochim. Acta* **401**, 169 (2003).
- ³⁶S. Lee, S. Y. Kwon, and H. J. Ham, *Jpn. J. Appl. Phys., Part 1* **50**, 11RG02 (2011).
- ³⁷R. Kremer, M. Cardona, E. Schmitt, J. Blumm, S. Estreicher, M. Sanati, M. Bockowski, I. Grzegory, T. Suski, and A. Jezowski, *Phys. Rev. B* **72**, 075209 (2005).
- ³⁸M. Sanati and S. K. Estreicher, *J. Phys.: Condens. Matter* **16**, L327 (2004).
- ³⁹E. Sichel and J. Pankove, *J. Phys. Chem. Solids* **38**, 330 (1977).
- ⁴⁰B. M. Foley, H. J. Brown-Shaklee, J. C. Duda, R. Cheaito, B. J. Gibbons, D. Medlin, J. F. Ihlefeld, and P. E. Hopkins, *Appl. Phys. Lett.* **101**, 231908 (2012).
- ⁴¹B. F. Donovan, C. J. Szejewski, J. C. Duda, R. Cheaito, J. T. Gaskins, C.-Y. P. Yang, C. Constantin, R. E. Jones, and P. E. Hopkins, *Appl. Phys. Lett.* **105**, 203502 (2014).
- ⁴²T. Beechem, J. C. Duda, P. E. Hopkins, and P. M. Norris, *Appl. Phys. Lett.* **97**, 061907 (2010).
- ⁴³Z. Tian, K. Esfarjani, J. Shiomi, A. S. Henry, and G. Chen, *Appl. Phys. Lett.* **99**, 053122 (2011).
- ⁴⁴T. Ruf, J. Serrano, M. Cardona, P. Pavone, M. Pabst, M. Krisch, M. D'Astuto, T. Suski, I. Grzegory, and M. Leszczynski, *Phys. Rev. Lett.* **86**, 906 (2001).
- ⁴⁵P. Klemens, *Proc. Phys. Soc. A* **68**, 1113 (1955).
- ⁴⁶Crystal constants are taken to be: $a = 3.189 \text{ \AA}$ and $c = 5.185 \text{ \AA}$.⁷¹ An average sound speed of 4929 m/s was used in line with Zou *et al.*⁴⁷
- ⁴⁷J. Zou, D. Kotchetkov, A. Balandin, D. Florescu, and F. H. Pollak, *J. Appl. Phys.* **92**, 2534 (2002).
- ⁴⁸The Pauling ionic radii for the various elements were as follows: Ga = 62, N = 146, Mg = 72, C = 260, H = 208, Si = 41, and O = 140 pm.
- ⁴⁹C. G. Van de Walle and J. Neugebauer, *J. Appl. Phys.* **95**, 3851 (2004).
- ⁵⁰M. Moss, *J. Appl. Phys.* **37**, 4168 (1966).
- ⁵¹K. Ohashi, *J. Phys. Soc. Jpn.* **24**, 437 (1968).
- ⁵²P. Carruthers, *Rev. Mod. Phys.* **33**, 92 (1961).
- ⁵³P. Carruthers, *Phys. Rev.* **114**, 995 (1959).
- ⁵⁴R. Berman, *Thermal Conduction in Solids*, Oxford Studies in Physics (Oxford University Press, 1976).
- ⁵⁵Y. Ni, S. Xiong, S. Volz, and T. Dumitrică, *Phys. Rev. Lett.* **113**, 124301 (2014).

- ⁵⁶K. Esfarjani, G. Chen, and H. Stokes, *Phys. Rev. B* **84**, 085204 (2011).
- ⁵⁷F. Yang and C. Dames, *Phys. Rev. B* **87**, 035437 (2013).
- ⁵⁸R. B. Dingle, *Proc. R. Soc. A* **201**, 545 (1950).
- ⁵⁹D. Florescu, V. Asnin, F. H. Pollak, A. Jones, J. Ramer, M. Schurman, and I. Ferguson, *Appl. Phys. Lett.* **77**, 1464 (2000).
- ⁶⁰V. Asnin, F. H. Pollak, J. Ramer, M. Schurman, and I. Ferguson, *Appl. Phys. Lett.* **75**, 1240 (1999).
- ⁶¹C. Luo, D. Clarke, and J. Dryden, *J. Electron. Mater.* **30**, 138 (2001).
- ⁶²C.-Y. Luo, H. Marchand, D. Clarke, and S. DenBaars, *Appl. Phys. Lett.* **75**, 4151 (1999).
- ⁶³W. Liu, A. A. Balandin, C. Lee, and H. Lee, *Phys. Status Solidi A* **202**, R135 (2005).
- ⁶⁴M. Kamano, M. Haraguchi, T. Niwaki, M. Fukui, M. Kuwahara, T. Okamoto, and T. Mukai, *Jpn. J. Appl. Phys., Part 1* **41**, 5034 (2002).
- ⁶⁵W. Liu and A. A. Balandin, *Appl. Phys. Lett.* **85**, 5230 (2004).
- ⁶⁶H. Shibata, Y. Waseda, H. Ohta, K. Kiyomi, K. Shimoyama, K. Fujito, H. Nagaoka, Y. Kagamitani, R. Simura, and T. Fukuda, *Mater. Trans.* **48**, 2782 (2007).
- ⁶⁷T. L. Bougher, L. Yates, C.-F. Lo, W. Johnson, S. Graham, and B. A. Cola, *Nanoscale Microscale Thermophys. Eng.* **20**, 22 (2016).
- ⁶⁸T. Westover, R. Jones, J. Y. Huang, G. Wang, E. Lai, and A. A. Talin, *Nano Lett.* **9**, 257 (2009).
- ⁶⁹C. T. Harris, "Development of a nanostructure thermal property measurement platform compatible with a transmission electron microscope," Ph.D. thesis, Massachusetts Institute of Technology, 2010.
- ⁷⁰C. Guthy, C.-Y. Nam, and J. E. Fischer, *J. Appl. Phys.* **103**, 064319 (2008).
- ⁷¹M. Leszczynski, T. Suski, P. Perlin, H. Teisseyre, I. Grzegory, M. Bockowski, J. Jun, S. Porowski, and J. Major, *J. Phys. D: Appl. Phys.* **28**, A149 (1995).